Spectrochimica Acta Part A: Molecular and Biomolecular Spectroscopy 323 (2024) 124926

Contents lists available at ScienceDirect

Spectrochimica Acta Part A:
Molecular and Biomolecular Spectroscopy

journal homepage: www.journals.elsevier.com/spectrochimica-acta-part-a-molecular-and-biomolecular-spectroscopy

Multiple pathways for lanthanide sensitization in self-assembled aqueous complexes

Amparo Navarro [a,1], Alvaro Ruiz-Arias [b,1], Francisco Fueyo-González [c,2], Carolina Izquierdo-García [c], Tomás Peña-Ruiz [a], Marta Gutiérrez-Rodríguez [c,d], Rosario Herranz [c], Juan M. Cuerva [e], Juan A. González-Vera [b,c,*], Angel Orte [b,*]

[a] Departamento de Química Física y Analítica, Universidad de Jaén, Facultad de Ciencias Experimentales, 23071 Jaén, Spain
[b] Nanoscopy-UGR Laboratory, Departamento de Fisicoquímica, Unidad de Excelencia de Química Aplicada a Biomedicina y Medioambiente, Facultad de Farmacia, University of Granada, Campus Cartuja, 18071, Granada, Spain
[c] Instituto de Química Médica (IQM-CSIC), Juan de la Cierva 3, 28006 Madrid, Spain
[d] PTI-Global Health CSIC, Juan de la Cierva 3, 28006 Madrid, Spain
[e] Departamento de Química Orgánica, Unidad de Excelencia de Química Aplicada a Biomedicina y Medioambiente, Facultad de Ciencias, University of Granada, Campus Fuentenueva, 18071 Granada, Spain

HIGHLIGHTS

- Lanthanide exhibit long PL lifetimes, facilitating time-resolved applications.
- Water-stable lanthanide luminophores are scarce.
- Despite water quenching, **PAnt** dynamically coordinates with Tb(III) and Eu (III)
- Spectroscopy and TD–DFT unveil sensitization mechanisms for Eu(III) and Tb (III)

GRAPHICAL ABSTRACT

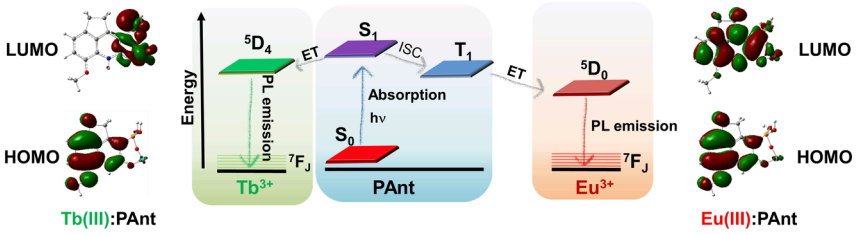

ARTICLE INFO

Keywords:
Lanthanides
Density functional calculations
Luminescence
Energy transfer
Photophysics

ABSTRACT

Lanthanide photoluminescence (PL) emission has attracted much attention for technological and bioimaging applications because of its particularly interesting features, such as narrow emission bands and very long PL lifetimes. However, this emission process necessitates a preceding step of energy transfer from suitable antennas. While biocompatible applications require luminophores that are stable in aqueous media, most lanthanide-based emitters are quenched by water molecules. Previously, we described a small luminophore, 8-methoxy-2-oxo-1,2,4,5-tetrahydrocyclopenta[*de*]quinoline-3-phosphonic acid (**PAnt**), which is capable of dynamically coordinating with Tb(III) and Eu(III), and its exchangeable behavior improved their performance in PL lifetime imaging microscopy (PLIM) compared with conventional lanthanide cryptate imaging agents. Herein, we report an in-depth photophysical and time-dependent density functional theory (TD–DFT) computational study that reveals different sensitization mechanisms for Eu(III) and Tb(III) in stable complexes formed in water. Understanding

* Corresponding authors at: Nanoscopy-UGR Laboratory, Departamento de Fisicoquímica, Unidad de Excelencia de Química Aplicada a Biomedicina y Medioambiente, Facultad de Farmacia, University of Granada, Campus Cartuja, 18071, Granada, Spain.
E-mail addresses: gonzalezvera@ugr.es (J.A. González-Vera), angelort@ugr.es (A. Orte).
[1] These authors contributed equally to this work.
[2] Current address: Department of Medicine, Translational Transplant Research Center, Immunology Institute. Icahn School of Medicine, Mount Sinai. New York, USA.

https://doi.org/10.1016/j.saa.2024.124926
Received 1 May 2024; Received in revised form 22 July 2024; Accepted 31 July 2024
Available online 3 August 2024

this unique behavior in aqueous media enables the exploration of different applications in bioimaging or novel emitting materials.

1. Introduction

Lanthanides have long fascinated researchers due to their unique properties and diverse applications, such as biological imaging and luminescent materials [1–5]. The electronic configuration of lanthanides involve the electrons in the 4f shell not contributing to the chemical bonding because they are shielded by the surrounding filled 5 s^2, 5 p^6, and 6 s^2 shells. Forbidden electronic transitions according to the Laporte selection rule facilitate long photoluminescence (PL) lifetimes and low absorbance [6,7]. Lanthanide spectra display sharp peaks, mostly independent of the surrounding enviroment, differing notably from broad fluorescence bands typical of organic fluorophores.

For their use as luminophores, indirect excitation via organic chromophores enhances lanthanide emission efficiency through the 'antenna effect' [8,9]. The donor state of the chromophore is usually a triplet state; however, energy transfer may occur via other pathways, such as a charge transfer state or a d-transition metal state [10]. One of the most direct and effective methods for sensitizing lanthanide emission is through the formation of soluble lanthanide complexes and cryptates, wherein the antenna chromophore may be directly involved. Additionally, various materials, including lanthanide-doped nanoparticles, metal–organic frameworks, and nanoclays offer promising avenues for luminescence sensitization [4,11–14]. Notably, their long PL lifetimes make these materials ideal for background-free imaging through time-gated analysis [2,3,15].

Different organic ligands capable of coordinating with lanthanides have been described, leading to the formation of antenna complexes in various solvents [12,16–21]. In such cases, a critical step is the actual complexation of the lanthanide ion, which typically exhibits slow kinetics, resulting in thermodinamically stable complexes formed after several weeks of incubation [22]. However, for biological applications, an ideally suited feature of luminescent species would be the rapid assembly of complexes in water, avoiding intricate preliminary synthesis steps. Few water-soluble lanthanide antennas have been reported, such as pyridine-2,6-dicarboxylate and pyridine-tetrazolate complexes [23,24], especially given that water deactivates lanthanide emission through vibrational energy transfer [11,23,25,26].

Our recent work introduced a compound, 8-methoxy-2-oxo-1,2-dihydrocyclopenta[*de*]quinoline-3-carboxylic acid, behaving as a luminescent sensor of biothiols in the study of human immune system cells [27]. Interestingly, the precursor compound **1** (Fig. 1) was found to coordinate and sensitize the emission of Tb(III) and Eu(III) in water [27]. Modification of **1** with a phosphonic acid resulted in the dye **PAnt** (Fig. 1), further enhancing complex stability with Tb(III) and Eu(III). The rapid formation of complexes in aqueous solution and the inherent exchagable nature of the dynamic equilibrium resulted in improved performance in PL lifetime imaging microscopy (PLIM) [28].

Consequently, we conducted and describe herein an in-depth photophysical study of such complexes. In this study, we employed full spectroscopic characterization and state-of-the-art time-dependent density functional theory (TD–DFT) calculations to study the photophysical properties and lanthanide sensitization mechanisms of self-assembled aqueous complexes of **PAnt** with Eu(III) and Tb(III); we compare their performance levels with those of the corresponding complexes formed with compound **1**. Interestingly, our results reveal that multiple pathways for lanthanide emission sensitization exist in self-assembled complexes.

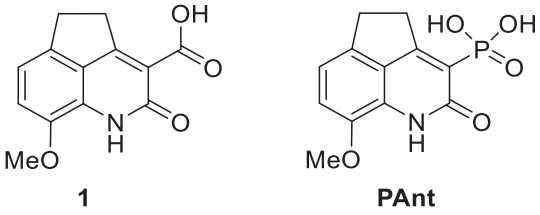

Fig. 1. Molecular structure of compounds **1** and **PAnt** (8-methoxy-2-oxo-1,2,4,5-tetrahydrocyclopenta[*de*]quinoline-3-phosphonic acid).

2. Materials and methods

General Methods. The synthesis of compounds **1** and **PAnt** was performed as described elsewhere [28,29]. All reagents were of commercial quality (molecular biology grade or HPLC grade). The solvents were dried and purified using standard methods before use.

UV–visible absorption spectra were collected using a Lambda 650 UV–visible spectrophotometer (PerkinElmer, Waltham, MA, USA). Steady-state fluorescence emission spectra were obtained using a Jasco FP-8300 spectrofluorometer (Jasco, Tokyo, Japan) with an integration time of 1 s/nm and excitation and emission slit widths of 2.5 nm. All spectra were corrected for background fluorescence by subtracting a blank scan of the solvent solution and spectrally corrected using certified fluorescence standards. Spectrally corrected excitation and emission spectra obtained at 77 K were collected using a Horiba Fluorolog QuantaMaster 8000 (Horiba Scientific, Japan) equipped with double monochromators and a cold finger cell holder for working under liquid nitrogen. Fluorescence quantum yields (Φ_F) of quinolin-2(1*H*)-one derivatives **1** and **PAnt** were determined in H_2O or CH_3CN and calculated using quinine sulfate dihydrate (in 0.1 M H_2SO_4) as a reference [30–32]. The concentrations of the sample and reference were set to ensure that the absorbance was less than 0.1 at identical excitation wavelengths. The following equation (1) was used to calculate the quantum yield:

$$\Phi_F = \frac{I_x \cdot A_r \cdot n_x^2}{I_r \cdot A_x \cdot n_r^2}\Phi_r \quad (1)$$

where *x* and *r* denote the sample and standard, respectively, *A* is the absorption at the excitation wavelength, *I* is the integrated fluorescence intensity, and *n* is the refractive index of the solvent.

PL emission spectra and lifetime measurements of lanthanide complexes were collected in a Varian Cary Eclipse Spectrofluorometer using the following conditions: excitation wavelength 320 nm; emission wavelength 545 nm for Tb(III) or 615 nm for Eu(III); excitation slit width 20.0 nm; emission slit width 20.0 nm; total decay time 5.0 ms; delay time 0.1 ms; gate time 0.2 ms; number of cycles 20; number of flashes 50; and PMT detector voltage 600 V. FT-IR spectra were collected on a Jasco FT/IR-460 Plus spectrometer equipped with an ATR module.

Computational methods. Full geometry optimizations of the S_0, S_1 and T_1 states of compounds **1** and **PAnt** were performed using the Gaussian16 (revision A.03) suite of programs [33] at the CAM-B3LYP3/6–31+G** [34] and ωB97xD/6–31+G** [35] levels of theory. The vibrational modes were calculated for S_0, S_1, and T_1 to verify that all vibrational frequencies are real. The polarizable continuum model (PCM) was used to implicitly describe the solvent as implemented in the Gaussian package [36–38]. Vertical electronic transitions were computed using TD-DFT calculations. The vertical electronic transitions $S_1 \rightarrow S_0$ in solution were calculated as the difference $ES_1(GS_1) - ES_0(GS_1)$, where $ES_1(GS_1)$ is the energy of the optimized S_1 state at its equilibrium geometry (state-specific solvation approach) [39] and $ES_0(GS_1)$ is the calculated energy of the S_0 state at the S_1 optimized state geometry and with the static solvation from the excited state [40].

The molecular geometry of the 1:1 complexes was optimized at the

CAM-B3LYP and ωB97xD levels of theory using the 6-31G** basis set for H, C, N, O, and P atoms and cc-PVDZ-DK3 for Eu and Tb lanthanides. The vibrational frequencies were also calculated to verify that all are real and that the lanthanide complexes are true minima. The infrared spectra calculated with CAM-B3LYP were scaled by 0.9631 [41].

3. Results and discussion

3.1. Photophysical properties of the antenna candidates

We conducted a photophysical study of compound **PAnt** and compared its properties with those of the parent compound **1**. The main results are listed in Table 1, whereas the corresponding fluorescence emission and absorption spectra are shown in the Supplementary Materials (SM, Figure S1). **PAnt** in water exhibited two absorption maxima at 310 and 345 nm in the blue region of the visible spectrum, similar to compound **1**. The reported molar absorption coefficients were in the same ranges as those of other lanthanide antennas reported previously [11,25,26,42]. Given that the two bands were well discriminated, according to the TD-DFT calculations, they were assigned to two possible transitions from the singlet ground electronic state (S_0) to the electronic state S_1 or S_2: $S_0 \rightarrow S_1$ or $S_0 \rightarrow S_2$.

In contrast, a single fluorescence emission band was detected, independent of the excitation wavelength, confirming direct emission from the first excited singlet state. The quantum yields obtained (using $\lambda_{ex} = 320$ and 350 nm) for these compounds were larger in water than in other solvents, such as acetonitrile; the yields were in the same range as those reported for other quinolin-2(1*H*)-ones [26]. To assign the electronic transitions to the observed absorption and emission bands, DFT and TD–DFT calculations were performed at the TD-CAM-B3LYP/6–31+G** and TD-ωB97xD/6–31+G** levels of theory for compounds **1** and **PAnt** in water solution. Two functionals were used to check the consistency of the theoretical predictions. Similar results were obtained using both functionals, so only those with TD-CAM-B3LYP will be discussed here while those with TD-ωB97xD are reported in the SM. Fig. 2 shows the experimental absorption spectrum of compounds **1** and **PAnt** along with the theoretical oscillator strength of the vertical electronic transitions ($\lambda^{calc}_{vert\text{-}ab}$) collected in Table 2. The weak bands observed around 345 and 373 nm in compounds **1** and **PAnt** could be assigned to the $S_0 \rightarrow S_1$ transition calculated at 318 and 309 nm, respectively, for which a low oscillator strength was predicted ($f \sim 0.06$–0.07). The stronger bands observed at 310 and 320 nm in **1** and **PAnt**, respectively, could be assigned to the $S_0 \rightarrow S_2$ transition calculated at 284 nm (**1**) and 276 nm (**PAnt**) in concordance with the higher oscillator strength predicted for them ($f \sim 0.34$–0.29). The $S_0 \rightarrow S_1$ transition involves HOMO and LUMO molecular orbitals, and from HOMO-1 to LUMO in the case of $S_0 \rightarrow S_2$, with large contributions of these molecular orbitals in both cases (~90 %). For compound **1**, three rotamers were found for the carboxylic acid group, but they yielded very similar results (Tables 2 and S1–S4 in the SM). The molecular orbitals and optimized structures of the compounds are presented in Figures S2–S4.

Regarding the emission, the first excited state was optimized and the $S_1 \rightarrow S_0$ electronic transition was predicted at 503 nm (**1**) and 482 nm (**PAnt**), in good agreement with the experimental observations, with differences of approximately 0.3 and 0.1 eV for compounds **1** and **PAnt**, respectively, using TD-CAM-B3LYP (see Table S3 for TD-ωB97xD/6–31+G**). The continuous solvent model used was water because our interest was in self-assembly in aqueous solutions. Nevertheless, given that the antennas have protonable groups, we could not rule out the possibility that specific solvent effects could notably influence the final emission properties; thus, quantum chemical calculations including explicit solvent molecules could be required for a better estimation of the photophysical properties [43]. However, for the purpose of using compounds **1** and **PAnt** as lanthanide antennas, the calculated geometries and molecular orbitals without explicit solvent molecules provided sufficient information as a starting point.

Table 1
Photophysical properties of compounds **1** and **PAnt**.

Compd[a]	Solvent	λ^{max}_{abs} /nm	ε [b] /M^{-1} cm^{-1}	λ^{max}_{em} /nm	Φ_F [c]
1 [d]	CH_3CN	320, 375	4720	450	0.09
	H_2O	320, 373	5451	472	0.11
PAnt	CH_3CN	310, 350	9329	436	0.08
	H_2O	310, 345	8434	441	0.14

[a] Measured in duplicate at a 167 μM concentration (**1**) and a 29 μM concentration (**PAnt**). [b] At the short wavelength maximum. [c] Quantum yields were calculated with reference to quinine sulfate (in 0.1 M H_2SO_4). [d] From reference [27].

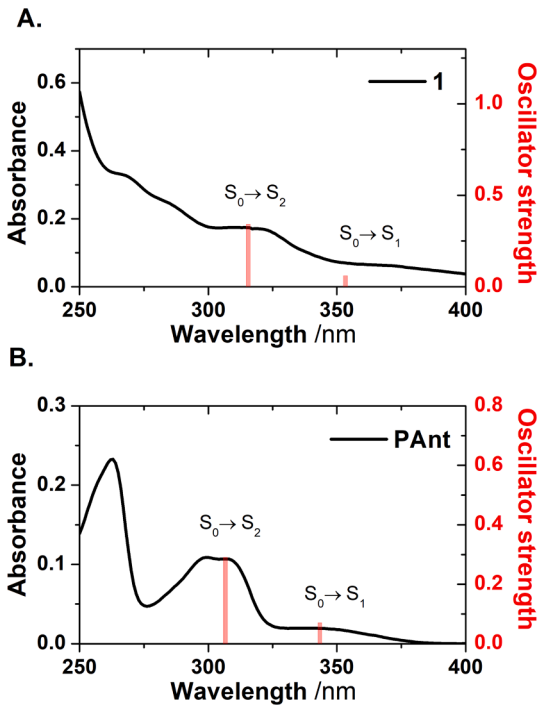

Fig. 2. Experimental absorption spectrum of compounds (A) **1** and (B) **PAnt** in aqueous solution, along with the oscillator strength of the vertical electronic transitions calculated in water solution at the TD-CAM-B3LYP/6–31+G** level of theory. The theoretical energies were scaled by a factor of 0.9.

3.2. Self-assembled complexes for effective lanthanide sensitization

The energy ranges of the absorption and emission spectra of **PAnt** made the compound suitable as a lanthanide ion antenna [6,25,42], similar to compound **1** [27]. These molecules must form stable self-assembled complexes to function as effective lanthanide antennas in water; this would allow optimal energy transfer and emission sensitization. In previous studies, we performed screenings to assess the sensitizing capabilities of **1** and **PAnt** toward different lanthanide ions and found that notable lanthanide PL emission was exhibited for Eu(III) and Tb(III) [27,28].

We then studied the stability and stoichiometry of the self-assembled complexes by applying different titrations. Fig. 3A and 3B show representative direct and inverse titrations of **PAnt** with Eu(III) (additional spectra for other direct and inverse titrations are shown in the SM, Figure S5 and S6). The formation of an effective self-assembled complex between **PAnt** and Eu(III) ions was evidenced by the almost complete quenching of the antenna emission at 445 nm due to energy transfer (99.6 ± 0.1 % quenching efficiency with 2 equivalents of Eu(III) added) and the appearance of the well-defined, narrow Eu(III) luminescence emission bands, peaking at 616 nm; this band corresponded to the $^5D_0 \rightarrow$

Table 2
Calculated photophysical properties of compounds **1** and **PAnt**. Maximum absorption (λ_{abs}^{max}) and emission wavelengths (λ_{em}^{max}) determined in aqueous solution. Calculated lowest-energy transition wavelengths ($\lambda_{vert\text{-}ab}^{calc}$ and $\lambda_{vert\text{-}em}^{calc}$) and oscillator strengths (*f*) for these transitions.[a]

Compd	λ_{abs}^{max} /nm (eV)	$\lambda_{vert\text{-}ab}^{calc}$ /nm (eV)	Transition	*f*	%Contribution	λ_{em}^{max} /nm (eV)	$\lambda_{vert\text{-}em}^{calc}$ /nm (eV)[b]	*f*
1	345 (3.59)	318 (3.90)	$S_0 \rightarrow S_1$	0.06	H→L (93)	441 (2.81)	503 (2.47)	0.10
	310 (4.00)	284 (4.37)	$S_0 \rightarrow S_2$	0.34	H-1 → L (90)			
PAnt	373 (3.32)	309 (4.00)	$S_0 \rightarrow S_1$	0.07	H→L (93)	472 (2.63)	482 (2.57)	0.11
	320 (3.87)	276 (4.50)	$S_0 \rightarrow S_2$	0.29	H-1 → L (86)			

[a] Calculations were performed at the CAM-B3LYP/6–31+G** level of theory in water.
[b] The emission corresponds to the $S_1 \rightarrow S_0$ transition.

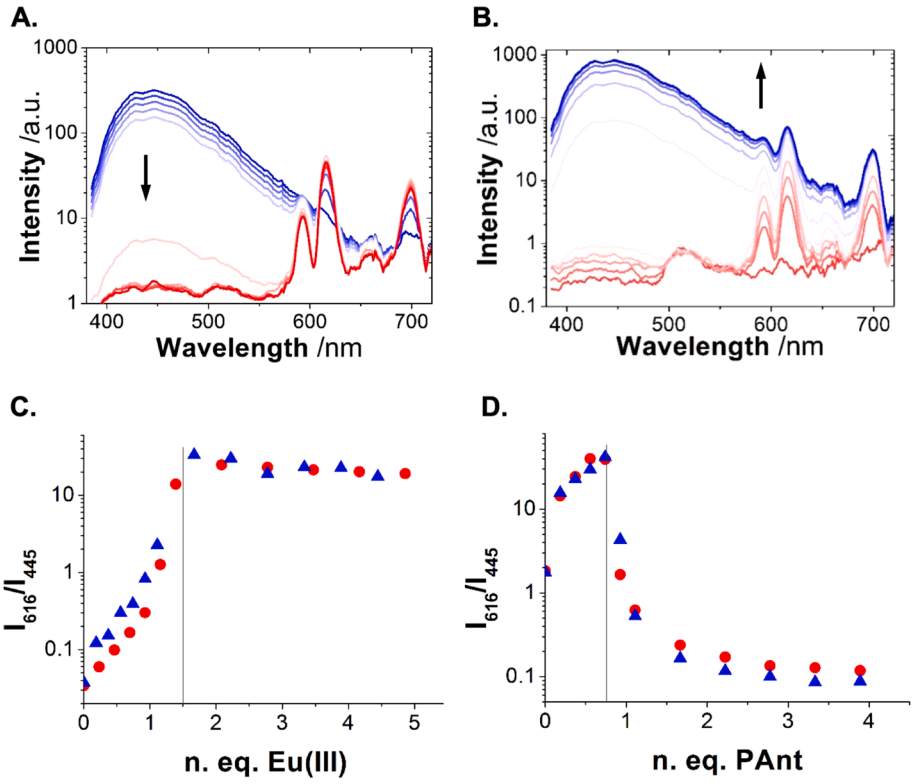

Fig. 3. A) Representative emission spectra (λ_{ex} = 320 nm) of direct titration of **PAnt** (27 μM) with increasing concentration of Eu(III) (from 0 to 86.2 μM) in aqueous solution. B) Representative emission spectra (λ_{ex} = 320 nm) of the inverse titration of Eu(III) (54 μM) with increasing concentration of **PAnt** (from 0 to 243 μM) in aqueous solution. The logarithmic scale in panels A) and B) was selected to visualize both the contribution of the antenna and the sensitized emission of the lanthanide. C) I_{616}/I_{445} ratios from direct titrations of **PAnt** at 54 μM (blue triangles) or 43 μM (red circles) with Eu(III). D) I_{616}/I_{445} ratios from inverse titrations of Eu(III) at 54 μM (blue triangles) or 43 μM (red circles) with **PAnt**.

$^7F_2$ transition in Eu(III). For the titration curve analysis, we focused our attention on the dual emission properties of the complexes, using the intensity ratio of the antenna fluorescence emission and the lanthanide-ion-sensitized PL emission as a normalized parameter to study the formation of emissive complexes because this ratio simultaneously reflects the efficiency of the antenna emission quenching, energy transfer, lanthanide sensitization and subsequent PL emission. Fig. 3C and 3D show the I_{616}/I_{445} ratio in direct and inverse titrations, respectively. The titrations with $EuCl_3$ at fixed concentrations of **PAnt** exhibited an increase in the ratio with increasing subequimolar ion concentration up to a 1:1 M ratio. There was a change in the growth slope, displaying a marked increase to saturation at a 1.5:1 (Eu(III):**PAnt**) proportion. Further addition of Eu(III) resulted in a decreased ratio. The inverse titrations showed consistent results (Fig. 3D). As the concentration of **PAnt** increased, the sensitized emission of Eu(III) increased up to an approximately equivalent amount of **PAnt**. Further addition of **PAnt** resulted in a marked decrease in the ratio. Interestingly, the data points for the two types of titrations—direct and inverse—perfectly matched each other (Figure S7) indicating that complete equilibrium was reached while measuring. The above behavior was rationalized as follows: when there is an excess of Eu(III), >99 % quenching of the compound **PAnt** emission indicates effective coordination in water and energy transfer. Entropy-controlled complexation must favor a 1:1 Eu(III)**:PAnt** complex in such situations. The stoichiometric excess of compound **PAnt** clearly resulted in a lower I_{616}/I_{445} ratio, indicating the presence of free antenna molecules.

To gain more insights into the actual stoichiometry and quantify association constants, we employed time-gated PL spectroscopy. This method focuses solely on the long-lived, sensitized emission of Eu(III), discarding the contribution from the antenna by applying a delayed detection time gate (Fig. 4B and S8 in the SM). We directly fitted these data to the general equations of 1:1 and 2:1 equilibrium binding models using the Bindfit platform (Fig. 4A) [44,45,46]. The 1:1 stoichiometry is characterized by the association constant, K_{11}. For the 2:1 stoichiometry, different models can be considered: i) statistical –a purely statistical model, in which the association constant for the second ligand molecule $K_{21} = K_{11}/4$ and the emission intensity is double that of the 1:1 complex; ii) non-cooperative –in which the relation between the

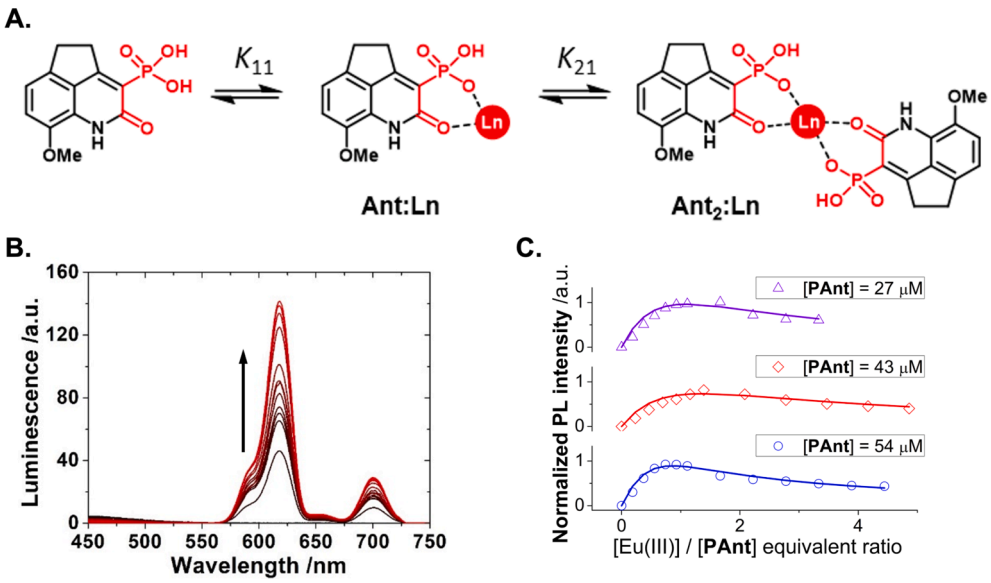

Fig. 4. A) Schematic of sequential 1:1 and 2:1 interactions used to fit the experimental titration data. As an example, the structure of **PAnt** is shown as the ligand. Similar considerations can be made with **1**. B) Time-gated PL emission spectra (λ_{ex} = 320 nm) for the titrations of **PAnt** (54 μM) with $EuCl_3$ (from 0 to 243 μM). The arrow indicates increasing concentrations of $EuCl_3$. C) Time-gated emission intensity at 616 nm from the titrations of different fixed concentrations of **PAnt** (54, 43, and 27 μM) and increasing concentrations of $EuCl_3$ from 0 to 5 equivalents. Lines represent the fitting to a 2:1 non-cooperative interaction model.

association constants is maintained at $K_{21} = K_{11}/4$, but the emission of the 2:1 complex is not necessarily doubled; iii) additive –a model with possible cooperativity, so that $K_{21} \neq K_{11}/4$, but keeping the emission intensity of the 2:1 complex as double that of the 1:1; and iv) full model –considering interaction cooperativity ($K_{21} \neq K_{11}/4$) and free relation between the emissions of the 1:1 and 2:1 complexes. To compare the statistical probability of each model and decide the most probable stoichiometry, we focused our attention on the Akaike's information criterion (AIC), recently introduced in the field of supramolecular chemistry [47]. AIC values can be calculated as $AIC = N \log(SS/N) + 2k$, where N represents the number of datapoints, SS denotes the sum of the squared residuals, and k signifies the number of adjustable parameters. The model with the lowest AIC value is considered the most likely. Additionally, Akaike weight values, denoted as w_i, were calculated as the normalized measure of evidence to favor the most probable model [47]. The global fits of the time-gated PL data (Fig. 4C) and the AIC criterion demonstrated that the most probable model matching the experimental data was the non-cooperative 2:1 stoichiometry (see SM and Table S7 for details). The K_{11} value obtained from the global fits was $(4.0 \pm 1.2) \times 10^4\ M^{-1}$, corresponding to a dissociation constant of 25 ± 8 μM. This model implies that the association constant for the 2:1 interaction was $(9.9 \pm 3.2) \times 10^3\ M^{-1}$. During these titrations, the 2:1 complexes appeared at low concentrations of Eu(III) added; however, an excess of lanthanide ions favored 1:1 stoichiometry interactions due to entropic considerations. The existence of (**PAnt**)$_2$:Eu(III) complexes peaked approximately at equimolar ratios of the ligand and the lanthanide ion, and their occurrence was consistently lower than 20 % (Figure S16). Notably, the emission decreased at high number of equivalents of Eu(III) added, indicating that the (**PAnt**)$_2$:Eu(III) complex is much more emissive than **PAnt**:Eu(III). This can be attributed to the more efficient protection of the lanthanide ion in the 2:1 complex from water molecules [48], but it could also be because the (**PAnt**)$_2$:Eu(III) complex has two antennas next to the Eu(III) and the sensitization process is more effective.

We followed a similar approach to investigate the interaction of **PAnt** with Tb(III). We performed direct and inverse titrations with $TbCl_3$, which were measured by steady-state fluorescence spectroscopy and time-gated PL spectroscopy (Fig. 5 and S9-S12 in the SM). In this case, the most probable model for the complex of **PAnt** with Tb(III) was the statistical 2:1 (Table S7 and SM for further details). The K_{11} value was $(1.3 \pm 0.3) \times 10^4\ M^{-1}$, which corresponds to a dissociation constant of 77 ± 20 μM. Interestingly, for the titrations at low concentrations of **PAnt** (43 and 27 μM), the most significant model was the 1:1, due to the low amount of 2:1 complex formed.

Although the study of the interactions between compound **1** and Tb (III) ions through direct and inverse titrations showed the formation of self-assembled complexes in water, resulting in sensitized Tb(III) luminescence emission (Figures S13-S15), our experiments showed that Tb (III):**1** complexes were more labile than those formed with **PAnt**; thus, saturation was not reached in the direct titrations. The datasets of the titrations of ligand **1** with Tb(III) only supported a model with stoichiometry 1:1 and an association constant of $(5.6 \pm 0.9) \times 10^3\ M^{-1}$, corresponding to a dissociation constant of 180 ± 30 μM. The complex with ligand **1** was less stable than that formed with **PAnt**, due to the better complexation performance of the phosphonic acid group in **PAnt**.

We also measured the PL lifetime τ_{PL} values for the studied complexes of compounds **1** and **PAnt** with two equivalents of the lanthanide ions. For **PAnt**, the τ_{PL} values of the complexes formed with Eu(III) and Tb(III) were 0.307 ± 0.007 ms and 0.117 ± 0.003 ms, respectively [28]. The complex formed by **1** and Tb(III) exhibited a τ_{PL} value of 0.126 ± 0.007 ms. These τ_{PL} values were relatively low compared to other Eu(III) and Tb(III) cryptates, which present lifetimes of approximately 1 ms [25,48–50]. However, our complexes strikingly self-assembled in water, but even under saturation conditions, there were several coordination positions left uncovered at which vibration-driven quenching via interaction with water molecules was feasible, resulting in reduced τ_{PL} values. Interestingly, the τ_{PL} values in aqueous solution and in deuterated water (D_2O) provide an estimation of the number of water molecules in the coordination shell of the ion, due to the sensitivity of the lifetime to vibronic coupling with O–H groups [51]. By performing titrations at different H_2O:D_2O ratios and measuring τ_{PL}, the value of $\tau_{PL}(D_2O)$ can be estimated by extrapolation. The number of water molecules in the coordination shell can then be obtained as $q = A \cdot (\tau_{PL}(H_2O)^{-1} - \tau_{PL}(D_2O)^{-1})$. Using this method, we obtained an average value of 2.8 and 5.1 water molecules for **PAnt**:Eu(III) and **PAnt**:Tb(III), respectively (see SM for details on the estimations). Given the larger stability and higher-order species found for **PAnt**:Eu(III), these results are consistent with the dynamic nature of the complexes formed. It is

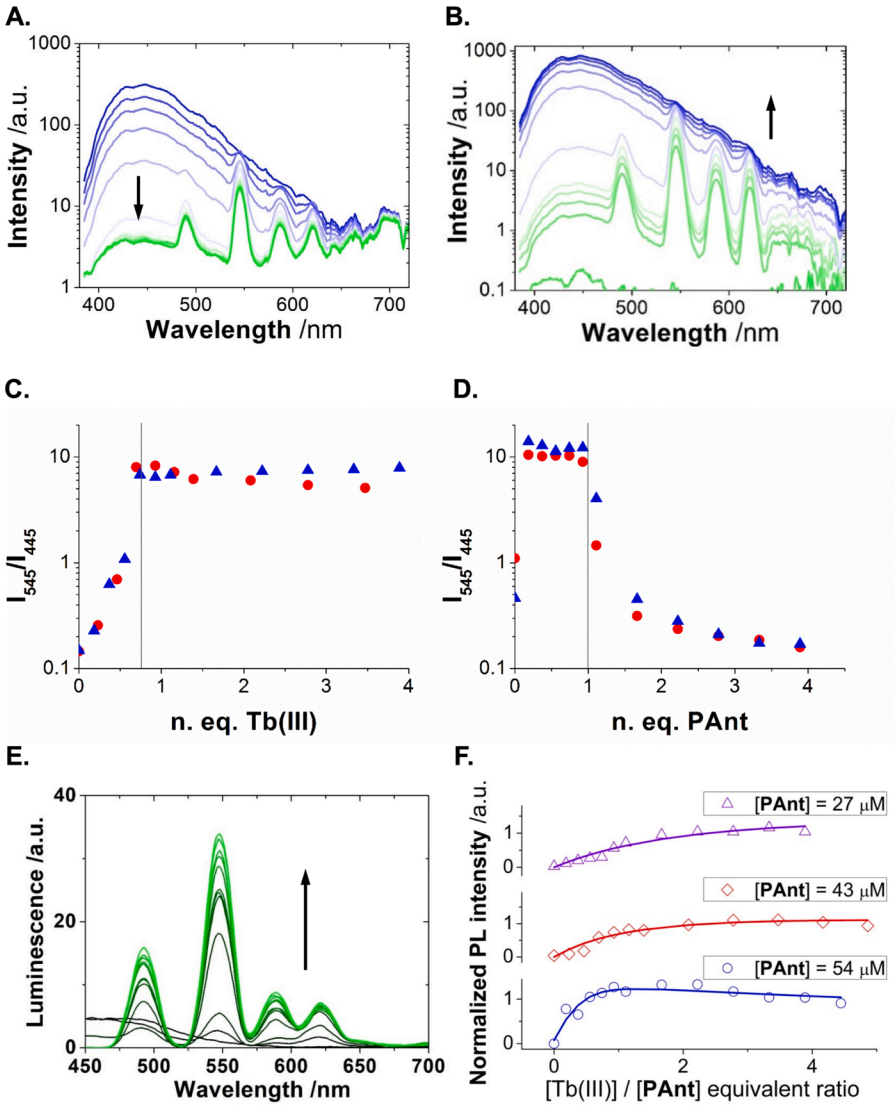

Fig. 5. A) Representative emission spectra (λ_{ex} = 320 nm) of direct titration of **PAnt** (27 μM) with increasing concentration of Tb(III) (from 0 to 86.2 μM) in aqueous solution. B) Representative emission spectra (λ_{ex} = 320 nm) of the inverse titration of Tb(III) (54 μM) with increasing concentration of **PAnt** (from 0 to 243 μM) in aqueous solution. The logarithmic scale in panels A) and B) was selected to visualize both the contribution of the antenna and the sensitized emission of the lanthanide. C) I_{545}/I_{445} ratios from direct titrations of **PAnt** at 54 μM (blue triangles) or 43 μM (red circles) with Tb(III). D) I_{545}/I_{445} ratios from inverse titrations of Tb(III) at 54 μM (blue triangles) or 43 μM (red circles) with **PAnt**. E) Time-gated PL emission spectra (λ_{ex} = 320 nm) for the titrations of **PAnt** (43 μM) with $TbCl_3$ (from 0 to 215 μM). The arrow indicates increasing concentrations of $TbCl_3$. F) Normalized time-gated PL intensity at 545 nm from the titrations of different fixed concentrations of **PAnt** (54 μM, black; 43 μM, red; and 27 μM, blue symbols) and increasing concentrations of $TbCl_3$ from 0 to 5 equivalents. Lines represent the fitting to a 2:1 statistical interaction model.

important to note that these are average values and are concentration-dependent, although they provide a valid insight into the nature of the complexes. As mentioned above, these complexes show low τ_{PL} values compared to cryptates. However, the main advantage of our approach is that the size of the antenna **PAnt** is much smaller than that of previously described cryptates. Additionally, **PAnt** exhibits enhanced water solubility, strikingly allowing for lanthanide emission sensitization in such a polar solvent.

3.3. *Lanthanide sensitization occurs via triplet and singlet states*

Once we demonstrated the ability of **PAnt** to sensitize lanthanide luminescence, we investigated the photophysics of the antenna effect and rationalized our results through state-of-the-art TD–DFT calculations. We included in our study the complexes formed with parent compound **1** for mechanistic comparisons. Energy transfer from the antenna to the lanthanide ions usually occurs via a long-lived triplet state, which provides a sufficient survival time of the excited state for the transition to excited electronic states of the lanthanide ion to proceed [6]. Once the ligand is excited from the ground state S_0 to the excited state S_1 by energy absorption, it rapidly relaxes to the T_1 triplet state via intersystem crossing; this process is usually facilitated by the presence of heavy atoms [13], and then, energy may be transferred to the lanthanide ion via either a Dexter or a Förster energy transfer mechanism [6].

As a usual guideline, the energy of the antenna triplet state should be within a suitable 2500 cm^{-1} region with respect to the emitting levels of the lanthanide ions–$^5D_4$ for Tb(III) or $^5D_0$ for Eu(III)–to avoid back transfer to the triplet state, thereby enhancing the quantum yield of the emissive complex [6,52,53]. TD–DFT and the CAM-B3LYP functional, in particular, have been shown to be very efficient in determining electronic vertical transitions in similar chemical systems [54,55]. Hence, we used our theoretical calculation results to verify this fact by comparing the emitting level of the lanthanides and the T_1 level of the

luminophores. Table S5 in the SM presents a list of the energy levels for the S_0, S_1 and T_1 states of **1** and **PAnt** and the energy gaps with respect to the emitting levels of Eu(III) and Tb(III). The calculated T_1 energy levels of organic ligands **1** and **PAnt** were similar to those of other typical π-conjugated systems, such as anthracene and pyrene [56]. The energy gaps between the T_1 levels of the ligands $\Delta(T_1\text{-}S_0)$ and the $^5D_0$ level of Eu (III) were 2380 cm^{-1} for **1** and 2490 cm^{-1} for **PAnt**, clearly following the expected distribution; the triplet level energy lay approximately 2500 cm^{-1} above the lanthanide level energy, sufficient to avoid energy back transfer from the lanthanide to the ligand [6]. In contrast, when the triplet state was compared with the emitting level of Tb(III), $^5D_4$, it was slightly lower, approximately 700–800 cm^{-1} below the lanthanide level (see Table S5). This phenomenon could result in very inefficient energy transfer and sensitization of Tb(III) ions [56,57], although examples of effective energy transfer with small energy gaps between the T_1 state and the lanthanide emitting level have been reported [6,58]. In such cases, several other mechanisms have been proposed that lead to lanthanide sensitization. The important role of the excited singlet state, S_1, as the donor state for the lanthanide emitting level was highlighted [6,57,59], especially when the differences between the excited singlet and triplet states, $\Delta(S_1\text{-}T_1)$, were greater than 5000 cm^{-1} [59], as was the case for both compounds ($\Delta(S_1\text{-}T_1)$ = 8040 cm^{-1} for **1** and 9090 cm^{-1} for **PAnt**; see Table S5). Therefore, while energy transfer to Eu(III) could conventionally occur via the long-lived triplet state, sensitization of Tb(III) could proceed via a more interesting singlet-state-mediated mechanism (Fig. 6A). The $\Delta(S_1\text{-}T_1)$ energy gaps were experimentally obtained using Gd(III) as the lanthanide ion for complex formation. The excitation–emission spectra were collected at a low temperature of 77 K (see Figures S17 and Table S8). These conditions ensure emission from triple states [53]. The obtained $\Delta(S_1\text{-}T_1)$ energy gaps were 8016 and 8815 cm^{-1} for **1** and **PAnt**, respectively, in perfect agreement with TD-DFT results from CAM-B3LYP/6–31+G**. We also performed the calculations using TD-ωB97xD/6–31+G**, however larger differences were obtained, predicting values of 8199 and 8469 cm^{-1} for **1** and **PAnt**, respectively (see Table S6).

To obtain further insights into the photosensitization mechanisms for Eu(III) and Tb(III), the molecular geometry of the most prominent 1:1 complexes is optimized in water at the CAM-B3LYP/6-31G**/cc-PVDZ-DK3 level of theory (see Figs. 6 and S18). The use of DFT functionals with high amounts of Hartree–Fock (HF) exchange is recommended for studying the orbital transitions of antennas for organo-lanthanide complexes [60]. The percentage of HF exchange in CAMB3LYP was 19 % in the short range, whereas it was 65 % in the long range and orbital transitions. Interactions of antenna luminophores with the lanthanide ions must occur through the carbonyl (in **1**) and phosphonate groups (in **PAnt**). We confirmed this hypothesis via Fourier transform infrared (FTIR) spectroscopy by focusing on the disappearance of the C=O stretching band at approximately 1750 cm^{-1} upon coordination [13,61] and the effects on the phosphonic vibration bands between 1000 and 1300 cm^{-1} [62]. In addition, we correlated the experimental and calculated vibrational spectra (see SM and Figure S19–S22), which were obtained with specific improved DFT methods for computing vibrations in organometallic complexes [41].

Representing frontier molecular orbitals is a fundamental technique for understanding electron density localization and the nature of orbital transitions upon photoexcitation when a ligand–lanthanide complex forms. Fig. 6C shows the HOMO and LUMO computed at the ground state at the CAM-B3LYP/6–31+G** level of theory, which are involved in the main electronic transitions of Eu(III)**:PAnt** and Tb(III)**:PAnt** (see Figure S23 in the SM for molecular orbitals from HOMO–1 up to LUMO+1 and those of Tb(III):**1**). Importantly, for Tb(III)**:PAnt**, the HOMO was localized over the ligand, whereas the LUMO was localized over the lanthanide, indicating clear charge separation. Thus, the LUMO exhibited ligand-to-metal charge transfer (LMCT) features. This separation of the wavefunctions could promote the transfer of excited electrons of the ligand from the HOMO to the LUMO located over the

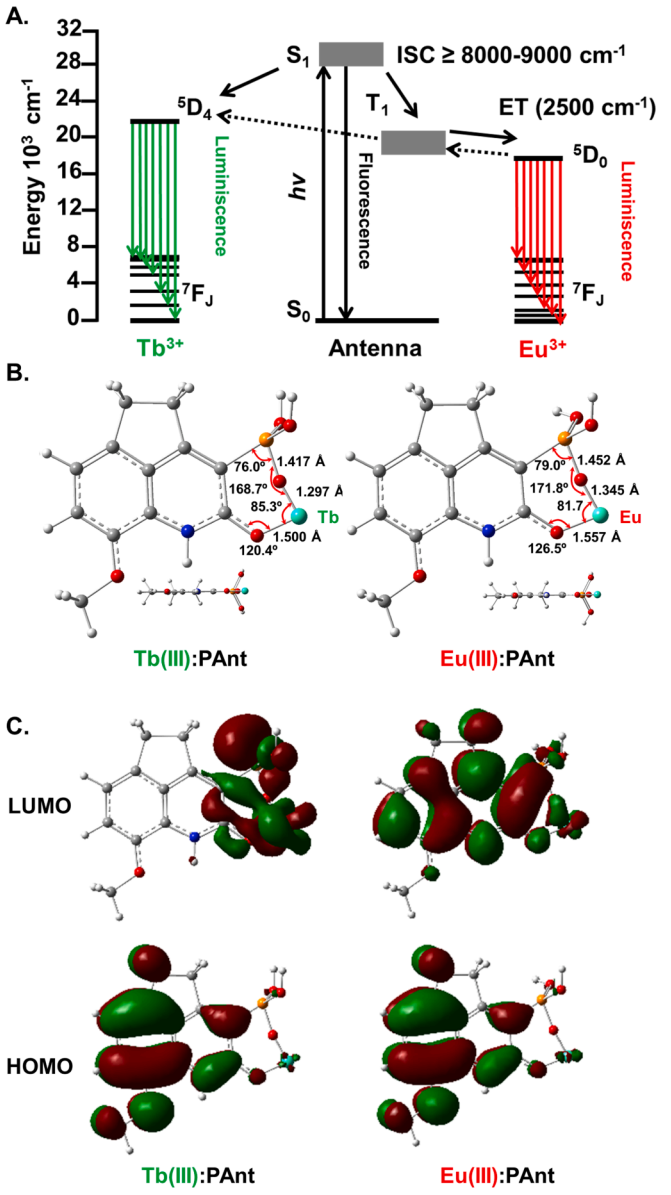

Fig. 6. A) Schematic representation of the energy levels of ligand compounds **1** and **PAnt**, calculated at the CAM-B3LYP/6–31+G** level of theory, in addition to the corresponding processes for sensitizing Eu(III) (right) through inter-system crossing (ISC) to the first triplet state, T_1, and subsequent energy transfer (ET) and for sensitizing Tb(III) (left) through LMCT via the singlet state, S_1. B) Selected geometrical parameters calculated for the ground state of compounds Tb(III)**:PAnt** and Eu(III)**:PAnt** in water. C) Frontier molecular orbitals in water calculated for the ground state. Calculations were performed at the CAM-B3LYP/6-31G**/cc-PVDZ-DK3 level of theory (0.02 a.u. iso-contour plots).

lanthanide through a Dexter energy transfer mechanism via an LMCT state [63]. This mechanism is a nonradiative mechanism of energy transfer from an electron donor (ligand) to an acceptor (lanthanide), which favors the efficiency of the antenna. However, that charge separation between HOMO and LUMO in Tb(III):**PAnt** does not appear as pronounced using ωB97xD/6–31+G** (see Figure S24). In contrast, for the Eu(III)**:PAnt** complex, there was an inversion of the molecular orbitals, and the LUMO exhibited ligand-localized charge (Fig. 6C); however, the LMCT state appeared at the LUMO+1 level (Figure S23). This finding supports the idea that charge transfer to the metal ion was not a requirement for Eu(III) sensitization, to the detriment of the Dexter energy transfer mechanism; thus, this sensitization could occur through

intersystem crossing to the antenna triplet state. In addition, the separation of the electron density was less pronounced in the case of the Tb(III):**1** complex (Figure S23), resulting in a lower efficiency of Tb(III) sensitization, as observed experimentally.

4. Conclusion

The in water self-assembled complexes of compound **PAnt** with both Eu(III) and Tb(III) have been suggested to be an important advance in PLIM imaging. In PLIM microscopy, the photostability of the dyes is an important hampering issue because very long lifetimes involve long acquisition times and thus long irradiation times. In contrast to other imaging lanthanide cryptates, the dynamic nature of the self-assembled complexes Eu(III)**:PAnt** and Tb(III)**:PAnt** intrinsically resulted in an exchangeable behavior that improved cellular PLIM imaging, even with the less efficient emission of the self-assembled complexes due to partial water quenching and the equilibrium-driven distribution of species [28].

The in-depth and comparative photophysical study of compounds **1** and **PAnt** showed that both efficiently form self-assembled complexes in water with Eu(III) and Tb(III), acting as antennas for the PL emissions of these cations. The complexes of antenna **PAnt** were almost one order of magnitude more stable than those of **1**, due to the better complexation performance of the phosphonic acid group of **PAnt** than that of the carboxylic acid of **1**. The binding isotherms revealed that the complexes formed with **PAnt** and Eu(III) or Tb(III) have a 2:1 stoichiometry. However, at working concentrations, the 1:1 complex becomes predominant. The experimental study was thoroughly complemented with computational data of compound **PAnt** and complexes Eu(III)**:PAnt** and Tb(III)**:PAnt**. Strikingly, such state-of-the-art TD–DFT calculations allowed us to conclude that whereas Eu(III) was sensitized through conventional triplet-state-fostered energy transfer, Tb(III) sensitization likely proceeded via LMCT from the excited singlet state. The new concept of exchangeable, self-assembled complexation in lanthanide luminescent agents for cellular imaging represents a completely different concept than established designs [2,3,8,25]. Likewise, this type of complexes are also relevant to other technological applications, such as obtaining water- or gel-based white-light emitters for novel emissive materials [28].

CRediT authorship contribution statement

Amparo Navarro: Writing – original draft, Visualization, Supervision, Software, Methodology, Investigation, Formal analysis, Conceptualization. **Alvaro Ruiz-Arias:** Writing – review & editing, Visualization, Investigation. **Francisco Fueyo-González:** Writing – review & editing, Resources, Methodology. **Carolina Izquierdo-García:** Writing – review & editing, Resources, Methodology. **Tomás Peña-Ruiz:** Writing – review & editing, Software, Methodology, Investigation, Formal analysis. **Marta Gutiérrez-Rodríguez:** Writing – review & editing, Supervision, Resources, Methodology, Funding acquisition. **Rosario Herranz:** Writing – review & editing, Supervision, Resources, Methodology. **Juan M. Cuerva:** Writing – review & editing, Supervision, Resources, Project administration, Methodology, Funding acquisition. **Juan A. González-Vera:** Writing – review & editing, Writing – original draft, Visualization, Supervision, Resources, Project administration, Methodology, Investigation, Funding acquisition, Conceptualization. **Angel Orte:** Writing – original draft, Visualization, Supervision, Project administration, Methodology, Funding acquisition, Formal analysis, Data curation, Conceptualization.

Declaration of competing interest

The authors declare that they have no known competing financial interests or personal relationships that could have appeared to influence the work reported in this paper.

Data availability

Data will be made available on request.

Acknowledgements

This work was supported by grants PID2020-114256RB-I00 and PID2022-137214OB-C22 funded by Agencia Estatal de Investigacion (Spain) AEI/10.13039/501100011033; grants P21_00212, A-FQM-386-UGR20 and 2021/00627/001-FEDER_UJA_2020 funded by FEDER/Junta de Andalucía-Consejería de Universidad, Investigación e Innovación (Andalucía regional government, Spain); the diaRNAgnosis project funded by the European Union's Horizon 2020 research and innovation programme under the Marie Sklodowska-Curie grant agreement No 101007934, CSIC (Spain) grant 202180E073, and PAIDI-FQM-337, Universidad de Jaén (Spain). Funding for open access charge: Universidad de Granada / CBUA. A.R.-A. thanks the Ministerio de Educación y Formación Profesional (Spain) for the FPU Ph.D. scholarship. The authors also acknowledge the Centro de Servicios de Informática y Redes de Comunicaciones (CSIRC) (Universidad de Granada, Spain) for providing the computing time and the Centro de Intrumentación Científica (CIC) (Universidad de Granada, Spain) for support with measurements at 77 K. The authors thank Prof. Juan M. Herrera for providing Gd(III) salts.

Appendix A. Supplementary data

Supplementary data to this article can be found online at https://doi.org/10.1016/j.saa.2024.124926.

References

[1] J. Yu, D. Parker, R. Pal, R.A. Poole, M.J. Cann, A Europium Complex That Selectively Stains Nucleoli of Cells, J. Am. Chem. Soc. 128 (2006) 2294–2299, https://doi.org/10.1021/ja056303g.
[2] J.C. Bunzli, Lighting up cells with lanthanide self-assembled helicates, Interface Focus 3 (2013) 20130032, https://doi.org/10.1098/rsfs.2013.0032.
[3] J.H.S.K. Monteiro, Recent Advances in Luminescence Imaging of Biological Systems Using Lanthanide(III) Luminescent Complexes, Molecules 25 (2020) 2089, https://doi.org/10.3390/molecules25092089.
[4] X. Zhu, X. Wang, H. Zhang, F. Zhang, Luminescence Lifetime Imaging Based on Lanthanide Nanoparticles, Angew. Chem. Int. Ed. 61 (2022) e202209378, https://doi.org/10.1002/anie.202209378.
[5] B.C. Roy, T.S. Mahapatra, Recent advances in the development of europium(iii) and terbium(iii)-based luminescent supramolecular metallogels, Soft Matter 19 (2023) 1854–1872, https://doi.org/10.1039/D2SM00999D.
[6] J.-C.-G. Bünzli, S.V. Eliseeva, Basics of Lanthanide Photophysics, in: P. Hänninen, H. Härmä (Eds.), Lanthanide Luminescence: Photophysical, Analytical and Biological Aspects, Springer, Berlin Heidelberg, Berlin, Heidelberg, 2011, pp. 1–45, https://doi.org/10.1007/4243_2010_3.
[7] W.D. Horrocks, Jr., M. Albin, Lanthanide Ion Luminescence in Coordination Chemistry and Biochemistry, Prog. Inorg. Chem. (1984) 1–104, https://doi.org/10.1002/9780470166321.ch1.
[8] G. Muller, Luminescent chiral lanthanide(III) complexes as potential molecular probes, Dalton Trans. 2009 (2009) 9692–9707, https://doi.org/10.1039/b909430j.
[9] J.B. Lamture, Z.H. Zhou, A.S. Kumar, T.G. Wensel, Luminescence Properties of Terbium(III) Complexes with 4-Substituted Dipicolinic Acid Analogs, Inorg. Chem. 34 (1995) 864–869, https://doi.org/10.1021/ic00108a017.
[10] J.-C.-G. Bünzli, S.V. Eliseeva, Intriguing aspects of lanthanide luminescence, Chem. Sci. 4 (2013) 1939–1949, https://doi.org/10.1039/c3sc22126a.
[11] M.H.V. Werts, Making sense of lanthanide luminescence, Sci. Prog. 88 (2005) 101–131, https://doi.org/10.3184/003685005783238435.
[12] S.N. Zhao, G. Wang, D. Poelman, P.V. Voort, Luminescent Lanthanide MOFs: A Unique Platform for Chemical Sensing, Materials 11 (2018) 572, https://doi.org/10.3390/ma11040572.
[13] A. Balamurugan, A.K. Gupta, R. Boomishankar, M. Lakshmipathi Reddy, M. Jayakannan, Heavy Atom Effect Driven Organic Phosphors and Their Luminescent Lanthanide Metal-Organic Frameworks, ChemPlusChem 78 (2013) 737–745, https://doi.org/10.1002/cplu.201300121.
[14] G. Du, L. Guo, L. Zhou, X. Pu, D. Zhao, H. Li, Boosting the Luminescence of a Europium(III)–β-Diketonate Complex–Nanoclay Aqueous Solution by Acetylcholine, Inorg. Chem. 63 (2024) 5982–5988, https://doi.org/10.1021/acs.inorgchem.4c00044.
[15] E. Garcia-Fernandez, S. Pernagallo, J.A. González-Vera, M.J. Ruedas-Rama, J. J. Díaz-Mochón, A. Orte, Time-Gated Luminescence Acquisition for Biochemical

Sensing: miRNA Detection, in: B. Pedras (Ed.), Fluorescence in Industry, Springer International Publishing, Cham, 2019, pp. 213–267, https://doi.org/10.1007/4243_2018_4.
[16] Y. Hasegawa, Y. Wada, S. Yanagida, H. Kawai, N. Yasuda, T. Nagamura, Polymer thin films containing Eu(III) complex as lanthanide lasing medium, Appl. Phys. Lett. 83 (2003) 3599–3601, https://doi.org/10.1063/1.1616207.
[17] Y. Kitagawa, R. Ohno, T. Nakanishi, K. Fushimi, Y. Hasegawa, Visible luminescent lanthanide ions and a large pi-conjugated ligand system shake hands, Phys. Chem. Chem. Phys. 18 (2016) 31012–31016, https://doi.org/10.1039/c6cp06294f.
[18] W.S. Lo, J. Zhang, W.T. Wong, G.L. Law, Highly luminescent Sm(III) complexes with intraligand charge-transfer sensitization and the effect of solvent polarity on their luminescent properties, Inorg. Chem. 54 (2015) 3725–3727, https://doi.org/10.1021/acs.inorgchem.5b00331.
[19] C. Xu, Photophysical properties of lanthanide complexes with 5-nitro-1,10-phenanthroline, Monatsh. Chem. 141 (2010) 631–635, https://doi.org/10.1007/s00706-010-0308-2.
[20] N.S. Kariaka, V.A. Trush, V.V. Dyakonenko, S.V. Shishkina, S.S. Smola, N. V. Rusakova, et al., New Luminescent Lanthanide Tetrakis-Complexes $NEt_4[LnL_4]$ Based on Dimethyl-N-Benzoylamidophosphate, ChemPhysChem 23 (2022) e202200129, https://doi.org/10.1002/cphc.202200129.
[21] D.E. Barry, D.F. Caffrey, T. Gunnlaugsson, Lanthanide-directed synthesis of luminescent self-assembly supramolecular structures and mechanically bonded systems from acyclic coordinating organic ligands, Chem. Soc. Rev. 45 (2016) 3244–3274, https://doi.org/10.1039/C6CS00116E.
[22] J. Moreau, E. Guillon, J.-C. Pierrard, J. Rimbault, M. Port, M. Aplincourt, Complexing Mechanism of the Lanthanide Cations Eu^{3+}, Gd^{3+}, and Tb^{3+} with 1,4,7,10-Tetrakis(carboxymethyl)-1,4,7,10-tetraazacyclododecane (dota)—Characterization of Three Successive Complexing Phases: Study of the Thermodynamic and Structural Properties of the Complexes by Potentiometry, Luminescence Spectroscopy, and EXAFS, Chem. Eur. J. 10 (2004) 5218–5232, https://doi.org/10.1002/chem.200400006.
[23] M.R. George, C.A. Golden, M.C. Grossel, R.J. Curry, Modified Dipicolinic Acid Ligands for Sensitization of Europium(III) Luminescence, Inorg. Chem. 45 (2006) 1739–1744, https://doi.org/10.1021/ic051461u.
[24] N. Wartenberg, O. Raccurt, E. Bourgeat-Lami, D. Imbert, M. Mazzanti, Multicolour Optical Coding from a Series of Luminescent Lanthanide Complexes with a Unique Antenna, Chem. Eur. J. 19 (2013) 3477–3482, https://doi.org/10.1002/chem.201203657.
[25] D. Parker, J.D. Fradgley, K.L. Wong, The design of responsive luminescent lanthanide probes and sensors, Chem. Soc. Rev. 50 (2021) 8193–8213, https://doi.org/10.1039/d1cs00310k.
[26] F. Fueyo-González, E. Garcia-Fernandez, D. Martínez, L. Infantes, A. Orte, J. A. González-Vera, et al., Smart lanthanide antennas for sensing water, Chem. Commun. 56 (2020) 5484–5487, https://doi.org/10.1039/D0CC01725F.
[27] F. Fueyo-González, L. Espinar-Barranco, R. Herranz, I. Alkorta, L. Crovetto, M. Fribourg, et al., Self-Assembled Lanthanide Antenna Glutathione Sensor for the Study of Immune Cells, ACS Sens. 7 (2022) 322–330, https://doi.org/10.1021/acssensors.1c02439.
[28] A. Ruiz-Arias, F. Fueyo-González, C. Izquierdo-García, A. Navarro, M. Gutiérrez-Rodríguez, R. Herranz, et al., Exchangeable Self-Assembled Lanthanide Antennas for PLIM Microscopy, Angew. Chem. Int. Ed. 63 (2024) e202314595, https://doi.org/10.1002/anie.202314595.
[29] J.A. Gonzalez-Vera, F. Fueyo-Gonzalez, I. Alkorta, M. Peyressatre, M.C. Morris, R. Herranz, Highly solvatochromic and tunable fluorophores based on a 4,5-quinolimide scaffold: novel CDK5 probes, Chem. Commun. 52 (2016) 9652–9655, https://doi.org/10.1039/c6cc04566a.
[30] C. Wurth, M. Grabolle, J. Pauli, M. Spieles, U. Resch-Genger, Relative and absolute determination of fluorescence quantum yields of transparent samples, Nat. Protoc. 8 (2013) 1535–1550, https://doi.org/10.1038/nprot.2013.087.
[31] K. Rurack, M. Spieles, Fluorescence Quantum Yields of a Series of Red and Near-Infrared Dyes Emitting at 600–1000 nm, Anal. Chem. 83 (2011) 1232–1242, https://doi.org/10.1021/ac101329h.
[32] A.M. Brouwer, Standards for photoluminescence quantum yield measurements in solution (IUPAC Technical Report), Pure Appl. Chem. 83 (2011) 2213–2228, https://doi.org/10.1351/PAC-REP-10-09-31.
[33] M.J. Frisch, G.W. Trucks, H.B. Schlegel, G.E. Scuseria, M.A. Robb, J.R. Cheeseman, et al., Gaussian 16 Rev. C.01, Wallingford, CT, 2016.
[34] T. Yanai, D.P. Tew, N.C. Handy, A new hybrid exchange–correlation functional using the Coulomb-attenuating method (CAM-B3LYP), Chem. Phys. Lett. 393 (2004) 51–57, https://doi.org/10.1016/j.cplett.2004.06.011.
[35] J.-D. Chai, M. Head-Gordon, Long-range corrected hybrid density functionals with damped atom–atom dispersion corrections, Phys. Chem. Chem. Phys. 10 (2008) 6615–6620, https://doi.org/10.1039/B810189B.
[36] M. Cossi, N. Rega, G. Scalmani, V. Barone, Energies, structures, and electronic properties of molecules in solution with the C-PCM solvation model, J. Comp. Chem. 24 (2003) 669–681, https://doi.org/10.1002/jcc.10189.
[37] J. Tomasi, B. Mennucci, R. Cammi, Quantum Mechanical Continuum Solvation Models, Chem. Rev. 105 (2005) 2999–3094, https://doi.org/10.1021/cr9904009.
[38] R. Cammi, S. Corni, B. Mennucci, J. Tomasi, Electronic excitation energies of molecules in solution: state specific and linear response methods for nonequilibrium continuum solvation models, J. Chem. Phys. 122 (2005) 104513, https://doi.org/10.1063/1.1867373.
[39] R. Improta, V. Barone, G. Scalmani, M.J. Frisch, A state-specific polarizable continuum model time dependent density functional theory method for excited state calculations in solution, J. Chem. Phys. 125 (2006) 054103, https://doi.org/10.1063/1.2222364.
[40] G. Scalmani, M.J. Frisch, B. Mennucci, J. Tomasi, R. Cammi, V. Barone, Geometries and properties of excited states in the gas phase and in solution: Theory and application of a time-dependent density functional theory polarizable continuum model, J. Chem. Phys. 124 (2006) 094107, https://doi.org/10.1063/1.2173258.
[41] M. Katari, E. Nicol, V. Steinmetz, G. van der Rest, D. Carmichael, G. Frison, Improved Infrared Spectra Prediction by DFT from a New Experimental Database, Chem. Eur. J. 23 (2017) 8414–8423, https://doi.org/10.1002/chem.201700340.
[42] E.G. Moore, A.P.S. Samuel, K.N. Raymond, From Antenna to Assay: Lessons Learned in Lanthanide Luminescence, Acc. Chem. Res. 42 (2009) 542–552, https://doi.org/10.1021/ar800211j.
[43] M.C. Gonzalez-Garcia, P. Herrero-Foncubierta, S. Castro, S. Resa, J.M. Alvarez-Pez, D. Miguel, et al., Coupled Excited-State Dynamics in N-Substituted 2-Methoxy-9-Acridones, Front. Chem. 7 (2019) 129 (1–13), https://doi.org/10.3389/fchem.2019.00129.
[44] www.supramolecular.org; Last accessed 04/2024.
[45] D. Brynn Hibbert, P. Thordarson, The death of the Job plot, transparency, open science and online tools, uncertainty estimation methods and other developments in supramolecular chemistry data analysis, Chem. Commun. 52 (2016) 12792–12805, https://doi.org/10.1039/C6CC03888C.
[46] P. Thordarson, Determining association constants from titration experiments in supramolecular chemistry, Chem. Soc. Rev. 40 (2011) 1305–1323, https://doi.org/10.1039/C0CS00062K.
[47] K. Ikemoto, K. Takahashi, T. Ozawa, H. Isobe, Akaike's Information Criterion for Stoichiometry Inference of Supramolecular Complexes, Angew. Chem. Int. Ed. 62 (2023) e202219059, https://doi.org/10.1002/anie.202219059.
[48] M. Li, Y. Zhou, Y. Yao, T. Gao, P. Yan, H. Li, Designing water-quenching resistant highly luminescent europium complexes by regulating the orthogonal arrangement of bis-beta-diketone ligands, Dalton Trans. 50 (2021) 9914–9922, https://doi.org/10.1039/d1dt00155h.
[49] W. Rochowiak, E. Kasprzycka, I.P. Assunção, U. Kynast, M. Lezhnina, Long-lifetime green-emitting Tb^{3+} complexes for bacterial staining, Austr. J. Chem. 75 (2022) 754–759, https://doi.org/10.1071/CH21315.
[50] W. Thor, Y. Wu, L. Wang, Y. Zhang, P.A. Tanner, K.-L. Wong, Charging and ultralong phosphorescence of lanthanide facilitated organic complex, Nat. Commun. 12 (2021) 6532, https://doi.org/10.1038/s41467-021-26927-z.
[51] A. Beeby, I.M. Clarkson, R.S. Dickins, S. Faulkner, D. Parker, L. Royle, et al., Non-radiative deactivation of the excited states of europium, terbium and ytterbium complexes by proximate energy-matched OH, NH and CH oscillators: an improved luminescence method for establishing solution hydration states, J. Chem. Soc., Perkin Trans. 2 (1999) 493–504, https://doi.org/10.1039/A808692C.
[52] L. Babetto, S. Carlotto, A. Carlotto, M. Rancan, G. Bottaro, L. Armelao, et al., Antenna triplet DFT calculations to drive the design of luminescent Ln^{3+} complexes, Dalton Trans. 49 (2020) 14556–14563, https://doi.org/10.1039/D0DT02624G.
[53] A.G. Cosby, J.J. Woods, P. Nawrocki, T.J. Sørensen, J.J. Wilson, E. Boros, Accessing lanthanide-based, in situ illuminated optical turn-on probes by modulation of the antenna triplet state energy, Chem. Sci. 12 (2021) 9442–9451, https://doi.org/10.1039/D1SC02148F.
[54] J. Hanuza, P. Godlewska, R. Lisiecki, W. Ryba-Romanowski, P. Kadłubański, J. Lorenc, et al., DFT study of electron absorption and emission spectra of pyramidal LnPc(OAc) complexes of some lanthanide ions in the solid state, Spectrochim. Acta A 196 (2018) 202–208, https://doi.org/10.1016/j.saa.2018.01.003.
[55] Y. Okayasu, J. Yuasa, Structure Determination of Europium Complexes in Solution Using Crystal-Field Splitting of the Narrow f–f Emission Lines, J. Phys. Chem. Lett. 12 (2021) 6867–6874, https://doi.org/10.1021/acs.jpclett.1c01885.
[56] Y. Hasegawa, Y. Kitagawa, T. Nakanishi, Effective photosensitized, electrosensitized, and mechanosensitized luminescence of lanthanide complexes, NPG Asia Mater. 10 (2018) 52–70, https://doi.org/10.1038/s41427-018-0012-y.
[57] E.V. Salerno, A.N. Carneiro Neto, S.V. Eliseeva, M.A. Hernández-Rodríguez, J. C. Lutter, T. Lathion, et al., Tunable Optical Molecular Thermometers Based on Metallacrowns, J. Am. Chem. Soc. (2022), https://doi.org/10.1021/jacs.2c04821.
[58] R.D. Archer, H. Chen, L.C. Thompson, Synthesis, Characterization, and Luminescence of Europium(III) Schiff Base Complexes1a, Inorg. Chem. 37 (1998) 2089–2095, https://doi.org/10.1021/ic960244d.
[59] E. Kasprzycka, V.A. Trush, V.M. Amirkhanov, L. Jerzykiewicz, O.L. Malta, J. Legendziewicz, et al., Contribution of Energy Transfer from the Singlet State to the Sensitization of Eu^{3+} and Tb^{3+} Luminescence by Sulfonylamidophosphates, Chem. Eur. J. 23 (2017) 1318–1330, https://doi.org/10.1002/chem.201603767.
[60] W. Thor, Y. Zhang, K.-L. Wong, P.A. Tanner, Orbital transitions: insight into energy transfer through an antenna for an organo-lanthanide complex, Chem. Commun. 57 (2021) 10727–10730, https://doi.org/10.1039/D1CC05246B.
[61] M.C. Mañas-Torres, C. Gila-Vilchez, J.A. González-Vera, F. Conejero-Lara, V. Blanco, J.M. Cuerva, et al., In situ real-time monitoring of the mechanism of self-assembly of short peptide supramolecular polymers, Mater. Chem. Front. 5 (2021) 5452–5462, https://doi.org/10.1039/D1QM00477H.
[62] M.C. Zenobi, C.V. Luengo, M.J. Avena, E.H. Rueda, An ATR-FTIR study of different phosphonic acids in aqueous solution, Spectrochim. Acta A 70 (2008) 270–276, https://doi.org/10.1016/j.saa.2007.07.043.
[63] P. Gawryszewska, V.M. Amirkhanov, V.A. Trush, D. Kulesza, J. Legendziewicz, The ligand-to-metal energy transfer and the role of Lewis base ligands and silver plasmons in emission of new type of lanthanide phosphors, J. Luminesc. 170 (2016) 340–347, https://doi.org/10.1016/j.jlumin.2015.06.039.